ACS APPLIED MATERIALS & INTERFACES

Research Article

www.acsami.org

Pentafluorophenoxy Boron Subphthalocyanine (F_5BsubPc) as a Multifunctional Material for Organic Photovoltaics

Graham E. Morse,[†,‡] Jeremy L. Gantz,[‡] K. Xerxes Steirer,[‡] Neal R. Armstrong,*[,‡] and Timothy P. Bender*[,†,§,∥]

[†]Department of Chemical Engineering & Applied Chemistry, University of Toronto, Toronto, Ontario M5S 3E5, Canada

[‡]Department of Chemistry and Biochemistry, University of Arizona, Tucson, Arizona 85721, United States.

[§]Department of Chemistry, University of Toronto, 80 St. George Street, Toronto, Ontario M5S 3H6, Canada

[∥]Department of Materials Science and Engineering, University of Toronto, 184 College Street, Toronto, Ontario M5S 3E4, Canada

Supporting Information

ABSTRACT: We have demonstrated that pentafluoro phenoxy boron subphthalocyanine (F_5BsubPc) can function as either an electron donor or an electron acceptor layer in a planar heterojunction organic photovolatic (PHJ OPV) cell. F_5BsubPc was incorporated into devices with the configurations ITO/MoO_3/F_5BsubPc/C_{60}/BCP/Al (F_5BsubPc used as an electron-donor/hole-transport layer) and ITO/MoO_3/Cl-BsubPc/F_5BsubPc/BCP/Al (F_5BsubPc used as an electron-acceptor/electron-transport layer). Each unoptimized device displayed open-circuit photopotentials (V_{oc}) close to or in excess of 1 V and respectrable power conversion efficiencies. Ultraviolet photoelectron spectroscopy (UPS) was used to characterize the band-edge offset energies at the donor/acceptor junctions. HOMO and LUMO energy level offsets for the F_5BsubPc/C_{60} heterojunction were determined to be ca. 0.6 eV and ca. 0.7 eV, respectively. Such offsets are clearly large enough to produce rectifying J/V responses, efficient exciton dissociation, and photocurrent production at the interface. For the Cl-BsubPc/F_5BsubPc heterojunction, the estimated offset energies were found to be ca. 0.1 eV. However, reasonable photovoltaic activity was observed, with photocurrent production coming from both BsubPc species layers. Incident and absorbed photon power conversion efficiencies (IPCE and APCE) showed that photocurrent production qualitatively tracked the absorbance spectra of the donor/acceptor heterojunctions, with some additional photocurrent activity on the low energy side of the absorbance band. We suggest that photocurrent production at higher wavelengths may be a result of charge-transfer species at the donor/acceptor interface. Cascade photovoltaics were also fabricated to expand on the understanding of the role of F_5BsubPc in such device architectures.

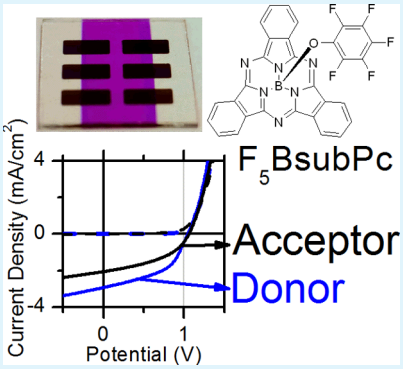

KEYWORDS: *photovoltaic, heterojunctions, solar, cells, boron, subphthalocyanines*

INTRODUCTION

The exploration of new classes of organic semiconductor materials continues to be of interest especially the exploration of new materials that can function as active layers in multiple device configurations such as organic light emitting diodes (OLEDs), organic photovoltaics (OPVs), and organic field effect transistors (OFETs), especially if there is a possibility that they can transport both holes and electrons with reasonable charge carrier mobilities.[1−3]

Boron subphthalocyanines (BsubPcs) are a class of strong magenta colored 14-π electron aromatic materials that have recently shown to be organic semiconductors in OPVs,[4−6] OLEDs,[7−9] and OFETs.[10] In these applications, BsubPcs were used as either an electron donor (hole transport material)[4,10] or an electron acceptor (electron transport material).[6] Included in this list is our demonstration that a series of fluorinated phenoxy boron subphthalocyanines, exemplified by pentafluoro phenoxy boron subphthalocyanine (F_5BsubPc), can function as both electron-transporting and electroluminescent materials in OLEDs.[7,8] More recently we have also measured the field dependent electron mobilities of the same series of fluorinated phenoxy boron subphthalocyanines and have shown their electron mobilities to be comparable to those seen for several other known electron-transporting materials (mobilities up to ca. 10^{-4} $cm^2/V{\cdot}s$ were observed).[11] We have shown that a novel series of phthalimido-BsubPcs can be used as electron-transporting emitters in OLEDs. The stable one-electron reduction and one-electron oxidation processes observed in solution for the phthalimido-BsubPcs suggest that they may be applicable as both electron- and hole-transporting materials.[12] Jones and coworkers have also recently shown that hole and electron transport is possible through a layer of chloro boron subphthalocyanine (Cl-BsubPc) in an OPVs.[13]

Received: September 24, 2013
Accepted: December 27, 2013
Published: December 27, 2013

   dx.doi.org/10.1021/am404179z | ACS Appl. Mater. Interfaces 2014, 6, 1515−1524

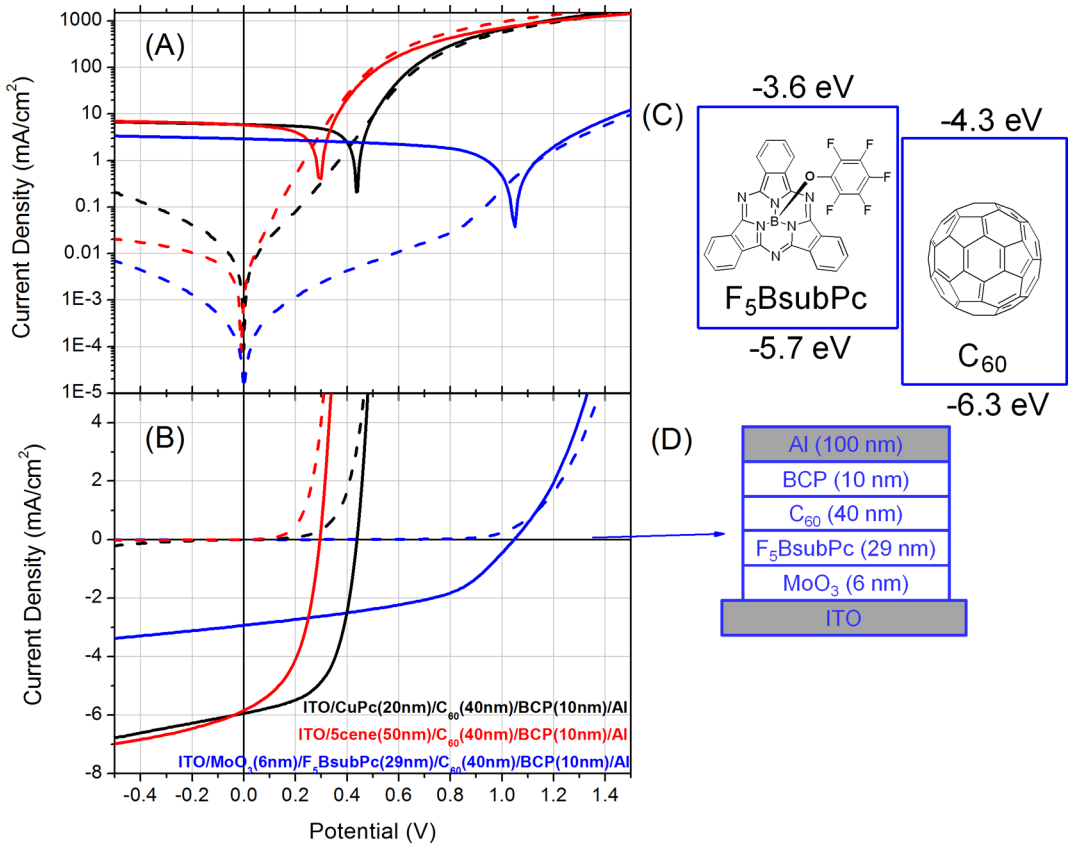

Figure 1. Log (A) and linear (B) dark and illuminated *J*/*V* plots for OPV devices fabricated with F_5BsubPc (blue line), CuPc (black line), or PEN (red line) as donor materials and C_{60} as an acceptor. (C) Schematic of the molecular structure of F_5BsubPc and its frontier molecular energy level alignment with C_{60}. (D) Device configuration of the F_5BsubPc/C_{60} OPV.

Recently, in this journal, our group has extensively reviewed the application of BsubPcs in organic electronic devices.[14] In that review we point out that the majority of the research concerning BsubPcs in organic electronic devices has been centered on the prototypical BsubPc: Cl-BsubPc. At the end of the review, we briefly mention preliminary results wherein we illustrate that F_5BsubPc, like Cl-BsubPc,[6] can function as either a electron-donor/hole-transporting layer or an electron-acceptor/electron-transporting layer in an OPV. We then go on to make the case for the expanded exploration of phenoxy-BsubPcs and other axially modified BsubPcs in organic electronic devices owing to the wide structure variation possible and the potential for systematically tuning the physical and electrophysical properties through synthetic variation.

Herein we present a comprehensive study of F_5BsubPc in planar heterojunction (PHJ) OPVs, F_5BsubPc being a representative from the more general class of materials, phenoxy-BsubPcs. We show that F_5BsubPc can function as an electron-donor material in a planar heterojunction (PHJ) OPV using C_{60} as the electron-accepting material. We also show that F_5BsubPc can function as an electron-acceptor material using Cl-BsubPc as the electron-donating material in an "all-BsubPc" PHJ OPV. Ultraviolet photoelectron spectroscopy (UPS) was used to estimate the ionization potentials for each layer in the PHJ OPV configurations, allowing for the estimation of the HOMO energy levels (and as a derivative thereof the LUMO energy levels) of the active materials and an estimation of the resulting impact of heterojunction formation between F_5BsubPc and either C_{60} or Cl-BsubPc on the energy levels.

RESULTS AND DISCUSSION

OPVs Based on F_5BsubPc/C_{60} Heterojunctions. BsubPcs are most commonly used in OPVs as electron-donor materials, the most common of which is Cl-BsubPc.[4,14] OPVs based on the pairing of Cl-BsubPc and C_{60} have shown good performance with the following device architecture: ITO/MoO_3 (5 nm)/Cl-BsubPc (10 nm)/C_{60} (33 nm)/BCP (8 nm)/Al (100 nm).[15,16] Therefore, F_5BsubPc was first evaluated as an alternative electron-donor material to Cl-BsubPc. F_5BsubPc/C_{60} devices were constructed as follows: ITO/MoO_3/F_5BsubPc/C_{60}/BCP/Al (Figure 1D). MoO_3 was used as an interlayer because it has been shown to enhance the efficiency of hole harvesting for a variety of electron donor materials.[16−19] The F_5BsubPc layer was varied in thickness from 17 to 37 nm, while C_{60} thickness was held constant at 40 nm. The devices consistently produced a large V_{oc} of ∼1 V (Table 1), larger than comparative devices constructed using electron donors such as copper phthalocyanine (CuPc) and pentacene (PEN, Figure 1, Table 1).[4] The F_5BsubPc layer thickness had a minimal impact on open circuit potential (V_{oc}, varying by ±0.05 V) and fill factors (FF, varying between 0.4 to 0.5) across the thickness range (Table 1). At 37 nm, the FF rapidly dropped to 33% and the *JV* curve resembled an s-kink, which we believe is caused by unbalanced charge transport at this thickness, leading to excessive recombination losses.[20−22] The power conversion efficiency was mainly dictated by the changes in current produced as a result of the change in exciton dissociation efficiency as the product of exciton diffusion length, L_D, and absorptivity, α, exceeded the optimal αL_D

dx.doi.org/10.1021/am404179z | ACS Appl. Mater. Interfaces 2014, 6, 1515−1524

Table 1. Summary of Device Optimization by Varying the F_5BsubPc Thickness in the Following Device Configuration: ITO/MoO_3 (6 nm)/F_5BsubPc/C_{60} (40 nm)/BCP (10 nm)/Al (100 nm)[a]

F_5BsubPc thickness (nm)	V_{oc} (V)	J_{sc} (mA/cm^2)	FF (%)	η (%)
17	1.07 ± 0.01	0.88 ± 0.16	48.6 ± 1.9	0.46 ± 0.10
27	1.02 ± 0.03	2.03 ± 0.39	46.2 ± 3.9	0.96 ± 0.22
29	1.05 ± 0.02	2.96 ± 0.59	48.2 ± 1.7	1.49 ± 0.27
32	1.05 ± 0.00	2.85 ± 0.63	43.9 ± 1.0	1.32 ± 0.27
37	1.03 ± 0.03	2.32 ± 0.32	33.4 ± 0.9	0.80 ± 0.16
reference CuPc (20 nm)	0.44 ± 0.02	5.94 ± 0.79	56.9 ± 2.5	1.49 ± 0.26
reference PEN (50 nm)	0.30 ± 0.01	5.84 ± 1.59	46.9 ± 1.6	0.82 ± 0.29

[a]Standard deviations for an average of at least eight 0.019 cm^2 devices are reported for each performance parameter. Two reference devices are shown for comparisons: ITO/CuPc (20 nm)/C_{60} (40 nm)/BCP (10 nm)/Al (100 nm) and ITO/PEN (50 nm)/C_{60} (40 nm)/BCP (10 nm)/Al (100 nm).

product.[23,24] It is also notable that the currents at zero bias are significantly lower than for the CuPc and PEN based OPVs, consistent with the idea that reverse saturation currents in the conventional Shockley equation describing the *JV* response of an OPV are dictated by the energy barrier between the transport HOMO of the donor and the transport LUMO of the acceptor and energy that is significantly higher for the BsubPcs.[25] Overall, the best performing device was found to be ITO/MoO_3 (6 nm)/F_5BsubPc (29 nm)/C_{60} (40 nm)/BCP (10 nm)/Al (100 nm) with an average power conversion efficiency of 1.5% (champion devices were observed with efficiencies as high as 2% (Figure 1A,B; Table 1)).

F_5BsubPc can clearly function as an electron donor when paired with C_{60}; however, F_5BsubPc also functions as an electron transporter.[7,11] Organic materials have been shown to form Schottky barriers with MoO_3 interfaces, producing photocurrent (organic material acting as electron acceptor).[26] Therefore, we were interested in locating the rectifying interface for exciton dissociation in the F_5BsubPc/C_{60} device(s) to prove the function of F_5BsubPc as an electron donor material. We sequentially "deconstructed" the F_5BsubPc/C_{60} device by making a series of new devices by first omitting the C_{60} layer and then the MoO_3 layer (Figure 2). We observed that the MoO_3/F_5BsubPc interface(s) do not adequately rectify and produced only a minimal photocurrent. A large V_{oc} > 1 V was however produced due to the large 2.1 eV bandgap of F_5BsubPc (Figure 2, blue line). This is similar to the large V_{oc} in MoO_3/C_{60} Schottky devices previously reported.[26] In contrast the F_5BsubPc/C_{60} device (without MoO_3, Figure 2, red line) produced similar J_{sc} current to its reference device (Figure 2, black line), albeit with an s-kink due to charge extraction limitations presumably caused by poor alignment of the ITO 4.7 eV work function with the low lying HOMO of F_5BsubPc (IP of 5.7 eV) in the absence of MoO_3. Thus, we can conclude that the F_5BsubPc/C_{60} interface is indeed the rectifying

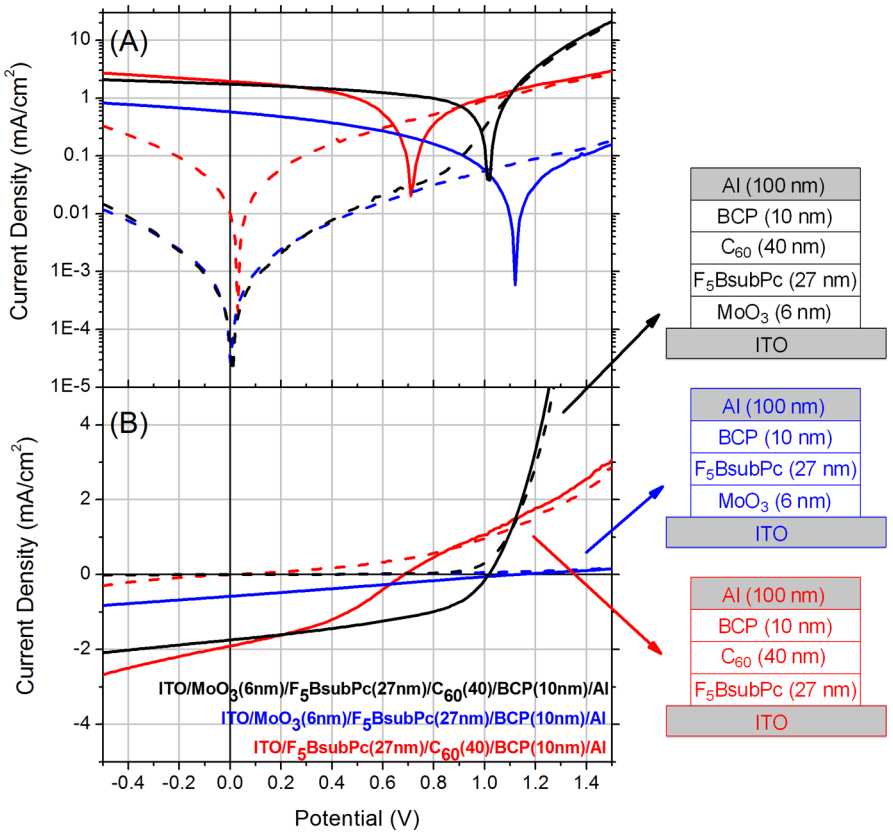

Figure 2. Log (A) and linear (B) dark and illuminated *J*/*V* plots for OPV devices: (black line) ITO/MoO_3 (6 nm)/F_5BsubPc (27 nm)/C_{60} (40 nm)/BCP (10 nm)/Al (100 nm), (red line) ITO/F_5BsubPc (27 nm)/C_{60} (40 nm)/BCP (10 nm)/Al (100 nm), and (blue line) ITO/MoO_3 (6 nm)/F_5BsubPc (27 nm)/BCP (10 nm)/Al (100 nm).

dx.doi.org/10.1021/am404179z | ACS Appl. Mater. Interfaces 2014, 6, 1515−1524

interface where photocurrent is generated in the ITO/MoO_3/F_5BsubPc/C_{60}/BCP/Al device(s), observations that are consistent with the UPS data outlined in the subsequent sections of this paper.

An IPCE plot for a representative ITO/MoO_3/F_5BsubPc/C_{60}/BCP/Al large area device is shown in Figure 3. A sharp

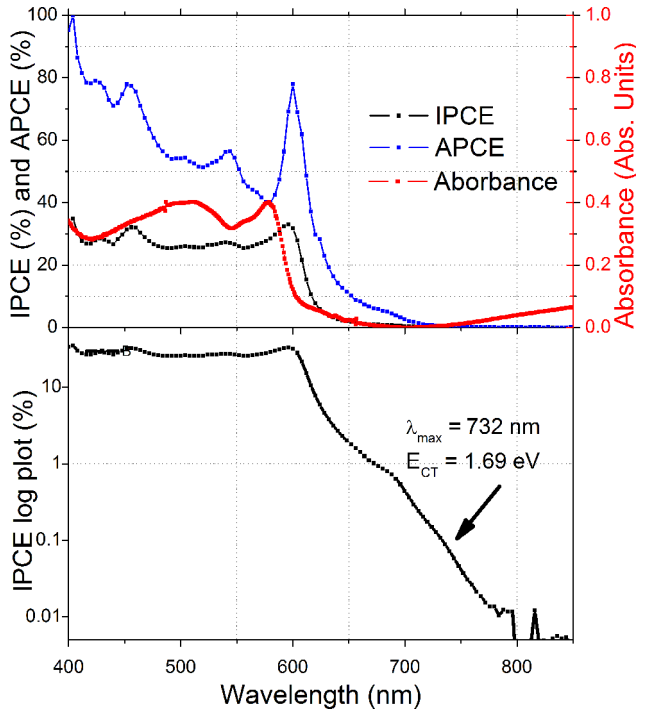

Figure 3. (top) IPCE (black line), APCE (blue line), and absorbance (red line) of an ITO/MoO_3 (6 nm)/F_5BsubPc (29 nm)/C_{60} (40 nm)/BCP (10 nm)/Al (100 nm) large area device. The absorbance spectrum coincides with what is expected of a combination of F_5BsubPc and C_{60}, the IPCE response peaks ca. 10−20 nm to the red of the main absorbance peak, suggesting that exciton dissociation is favored by excitation of a minority species at the F_5BsubPc/C_{60} heterojunction. (bottom) A plot of the log of IPCE versus wavelength for the same device.

increase in the IPCE spectra at ∼600 nm is seen with an IPCE response of 33% corresponding to the contribution to the photocurrent production from the absorption of light from F_5BsubPc. The F_5BsubPc/C_{60} device also shows a significant photoresponse from the absorption of light by C_{60} between 400 and 500 nm (Figure 3). The absorption is exclusively from C_{60}, since F_5BsubPc has an absorption minimum over that range. The devices maintain ∼30% IPCE throughout this absorption range. The J_{sc} estimated from the integration of the IPCE spectrum, normalized to the AM 1.5G spectral response, and the excitation lamp output,[27] was 1.81 mA/cm^2, which is lower than the measured value (3.1 mA/cm^2). For comparison, Cl-BsubPc (13 nm)/C_{60} (33 nm) devices are reported to have an IPCE of ∼45% at the Cl-BsubPc absorption maximum.[15] Photocurrent from a possible charge transfer (CT) complex between F_5BsubPc and C_{60} can be observed in the IPCE spectrum, at a wavelength of 732 nm, which is consistent with absorption from a CT state at 1.69 eV (Figure 3, bottom). Similar CT states have been previously observed in Cl-BsubPc/C_{60} planar or graded heterojunctions with IPCE contributions starting at 600 nm and tailing to 750 nm.[28,29] The energy of charge transfer states in OPV devices has recently been correlated to measured V_{oc}.[30] Applying this concept to the F_5BsubPc/C_{60} devices predicts an V_{oc} of 1.09 ± 0.07 V and in good agreement with our experimental measurements.

OPVs Based on Cl-BsubPc/F_5BsubPc Heterojunctions. In our previous work detailing the use of F_5subPc in OLEDs and in single carrier devices, we demonstrated that F_5BsubPc can act as an electron transporting and electroluminescent material.[7,8,11] In the preceding section, we outlined the pairing of F_5BsubPc with C_{60} wherein its role was as a hole transporter and light absorber. The frontier molecular orbitals of F_5BsubPc also suggest that it would be an effective material in OPVs as an electron acceptor if electron donor materials are selected with an appropriate energetic offset. For example, our UPS data outlined in the following sections of this paper suggest that F_5BsubPc can used as an acceptor material when paired with Cl-BsubPc (5.6 eV),[4] albeit with a relatively small band edge offset of ∼0.1 eV. There is literature precedence of "all-BsubPc" devices producing V_{oc} near 1 V with only 0.1−0.3 eV offset in their IP (0.2−0.6 eV offset in electron affinity values) and producing high power conversion efficiencies (2.7% and 4%).[6,31] We also selected pentacene (PEN) as an alternative electron-donating material for pairing with F_5BsubPc because of its lower IP (4.8 eV) and its significant HOMO offset versus F_5BsubPc (Figure 4).[32,33]

Devices with the configurations Al (100 nm)/BCP (8 nm)/F_5BsubPc (*x* nm)/Cl-BsubPc (10 nm)/MoO_3 (8 nm)/ITO and Al (100 nm)/BCP (8 nm)/F_5BsubPc (*x* nm)/PEN (50 nm)/ITO (Figure 4D) were thus constructed and evaluated as PHJ OPVs. Reasonable rectification was observed in the dark for both device configurations (Figure 4). The F_5BsubPc layer thickness was varied while the thicknesses of the PEN and Cl-BsubPc layers were held constant at 50 and 10 nm, respectively (according to best practices for each outlined in the literature).[4,34] Using F_5BsubPc as the electron transport layer, V_{oc} values of 0.95 and 1.05 V were observed for PHJ OPVs with PEN and Cl-BsubPc electron donors, respectively (Figure 4). The best thickness for the F_5BsubPc layer in the F_5BsubPc/Cl-BsubPc devices over the range tested was 40 nm, resulting in a J_{sc} of 2.1 mA/cm^2. For the PEN/F_5BsubPc devices the best thickness over the range tested was found to be 51 nm producing a J_{sc} of 0.73 mA/cm^2. The fill factors for each device were comparable at 43.2% and 41.8%, respectively and the best power conversion efficiencies for Cl-BsubPc/F_5BsubPc and PEN/F_5BsubPc devices were 0.94% and 0.28%, respectively (Table 2). The performance of larger area devices is summarized in the Supporting Information accompanying this paper.

In the case of the "all-BsubPc" Cl-BsubPc/F_5BsubPc device, IPCE measurements showed that absorption of wavelengths between 450 and 650 nm contributed to the photoresponse of the device (Figure 5). This narrow spectral response is not surprising and is a result of the near identical absorption profiles of the two active materials (Cl-BsubPc and F_5BsubPc). The highest photoresponse is observed at 596 nm with an IPCE of 47%. A second peak in the IPCE spectra is observed at 548 nm similar to the absorbance shoulder present for the BsubPcs. Charge transfer states are also observed at the onset of the IPCE plot (Figure 5, bottom). Here a peak is observed at 720 nm representing absorbance and photocurrent production from a CT state at 1.72 eV. Calculating the predicted V_{oc} using the correlation developed by Graham[30] suggests a value of 1.12 ± 0.07 V, once again in good agreement with our experimentally measured V_{oc}.

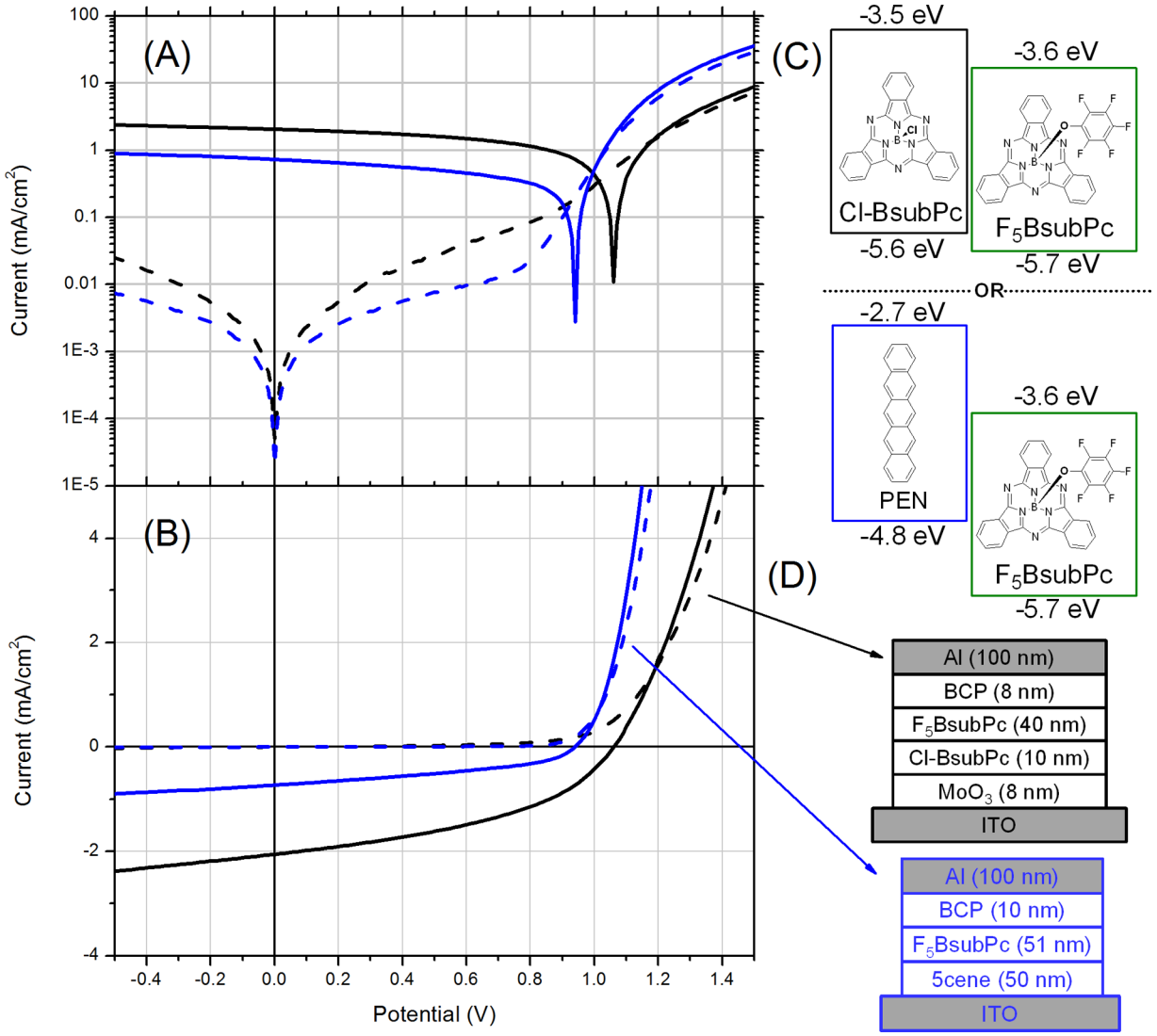

Figure 4. Log (A) and linear (B) dark and illuminated *J*/*V* plots for OPVs using F_5BsubPc as an acceptor and PEN (blue line) or Cl-BsubPc (black line) as donor materials. (C) Schematics of the molecular structure of F_5BsubPc and its frontier molecular energy level alignment with PEN and Cl-BsubPc. (D) The structure of the Cl-BsubPc/F_5BsubPc and the PEN/F_5BsubPc devices.

Table 2. Summary of Device Optimization by Varying the F_5BsubPc Thickness in the Following Device Configurations: ITO/PEN (50 nm)/F_5BsubPc/BCP (10 nm)/Al (100 nm) and ITO/MoO_3 (8 nm)/Cl-BsubPc (10 nm)/F_5BsubPc/BCP (10 nm)/Al (100 nm)[a]

F_5BsubPc thickness (nm)	V_{oc} (V)	J_{sc} (mA/cm²)	FF (%)	η (%)
PEN(50 nm)/F_5BsubPc				
29	0.82 ± 0.04	0.46 ± 0.09	40.8 ± 6.8	0.15 ± 0.01
38	0.89 ± 0.01	0.57 ± 0.09	42.7 ± 0.7	0.22 ± 0.03
51	0.94 ± 0.02	0.73 ± 0.13	41.4 ± 3.5	0.28 ± 0.05
Cl-BsubPc(10 nm)/F_5BsubPc				
20	0.98 ± 0.02	1.72 ± 0.52	45.1 ± 1.5	0.76 ± 0.24
30	0.98 ± 0.02	2.01 ± 0.66	43.7 ± 2.1	0.86 ± 0.28
40	1.06 ± 0.03	2.06 ± 0.71	43.2 ± 0.9	0.94 ± 0.33

[a]Standard deviations for an average of at least eight 0.019 cm² devices are reported for each performance parameter.

By integrating the IPCE spectra and normalizing it to the spectral output of our AM1.5G illumination source,[27] we estimate a device J_{sc} of 2.38 mA/cm², which is in good agreement with experimental observations (2.19 mA/cm²). By comparison to the F_5BsubPc/C_{60} device discussed above, an improvement from 33% to 47% in IPCE at 600 nm indicates an additional contribution from the Cl-BsubPc in the photoresponse. The IPCE performance of Cl-BsubPc/C_{60} devices in literature[15,29] and Cl-BsubPc/F_5BsubPc devices outlined herein are similar to a photoresponse of ~45% at 600 nm.

Finally, to probe the Cl-BsubPc/F_5BsubPc interface as the rectifying interface, we also deconstructed the ITO/MoO_3/Cl-BsubPc/F_5BsubPc/BCP/Al device. Schottky junction devices that lacked the F_5BsubPc layer were constructed (ITO/MoO_3/Cl-BsubPc/F_5BsubPc/BCP/Al). These Schottky junction devices lacked rectification (Figure S4, Supporting Information) similar to previous reports,[35] and therefore we can conclude that the Cl-BsubPc/F_5BsubPc interface must be the rectifying interface and F_5BsubPc must be acting as an electron acceptor, an observation that is consistent with the UPS data outlined below.

Band-Edge Energies for F_5BsubPc/C_{60} and Cl-BsubPc/F_5BsubPc Heterojunctions. We then moved to establish the

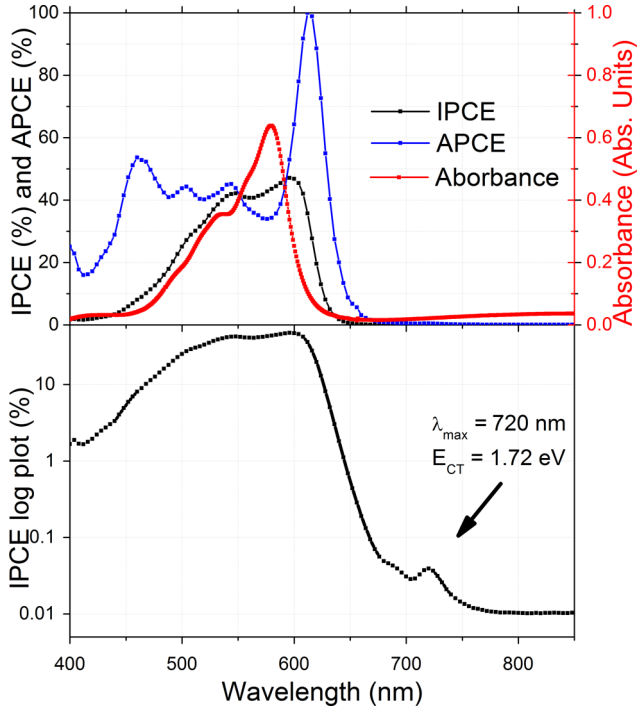

Figure 5. (top) IPCE (black line), APCE (blue line) (arbitrary units), and absorbance (red line) of the ITO/MoO_3 (8 nm)/Cl-BsubPc (10 nm)/F_5BsubPc (40 nm)/BCP (8 nm)/Al (100 nm) large area device. As for the F_5BsubPc/C_{60} OPVs, the absorbance spectrum is a composite of absorbance from both BsubPcs; the IPCE spectra suggest photocurrent production from minority forms of the BsubPcs at the F_5BsubPc/Cl-BsubPc heterojunction absorbing at near 615 nm. (bottom) A plot of the log of IPCE versus wavelength for the same device.

band-edge offsets for the frontier orbital energies for F_5BsubPc as an electron donor in heterojunctions with C_{60} as an electron acceptor, and for F_5BsubPc as an electron acceptor in heterojunctions with Cl-BsubPc as the electron donor. This was done to evaluate the offsets in transport HOMO and LUMO levels, which are believed to be necessary for efficient exciton dissociation and selective charge extraction.[4,23,36] Figure 6 shows the offsets in HOMO energies for the F_5BsubPc/C_{60} heterojunction, as estimated from UPS characterization of vacuum deposited thin films of the relevant materials, starting with a clean Au substrate.[37,38] Equivalent results were obtained with ITO substrates, but electronic equilibrium is easier to maintain during UPS experiments on Au substrates, using film thicknesses of each layer that are the same as those used in the above outlined devices. Above, we used thin layers of vacuum deposited MoO_3 to enhance hole collection in the devices,[17,18] and this was replicated for the UPS experiments on Au substrates. UPS data is shown in detail in Supporting Information for each heterojunction examined. We typically started with clean Au, added the MoO_3 layer at a device relevant thickness, followed by the donor layer also at its device relevant thickness, and then a few layers of the electron acceptor, up to its final device thickness. After correction for the significant local vacuum level shifts (as determined by shifts in the low kinetic energy region of the UPS spectra), especially for the F_5BsubPc/C_{60} interface, we found an offset in HOMO energies for F_5BsubPc and C_{60} of 0.6 eV. Assuming a transport bandgap for F_5BsubPc of 2.1 eV and a transport gap of ca. 2.0 eV for C_{60}, we estimate an offset in transport LUMO levels, $E^{LUMO}_{F_5} - E^{LUMO}_{C_{60}}$ = ca. 0.7 eV, which is more than sufficient to provide the driving force for exciton dissociation at the F_5BsubPc/C_{60} interface.[23] There are, in addition, adequate offsets in the HOMO and LUMO levels to provide the rectification and selective charge harvesting associated with planar heterojunction OPVs.[39−42]

Figure 7 shows the energetic offsets for the Cl-BsubPc/F_5BsubPc heterojunctions. The IP of F_5BsubPc is only ca. 0.1 eV larger than for Cl-BsubPc, and from the absorbance spectra of their thin films, the offset in transport LUMOs ($E^{LUMO}_{Cl\text{-}BsubPc} - E^{LUMO}_{F_5BsubPc}$) is estimated to be ca. 0.1 eV, suggesting a lower driving force for exciton dissociation and offsets in the transport HOMO and LUMO energies, which might make rectification

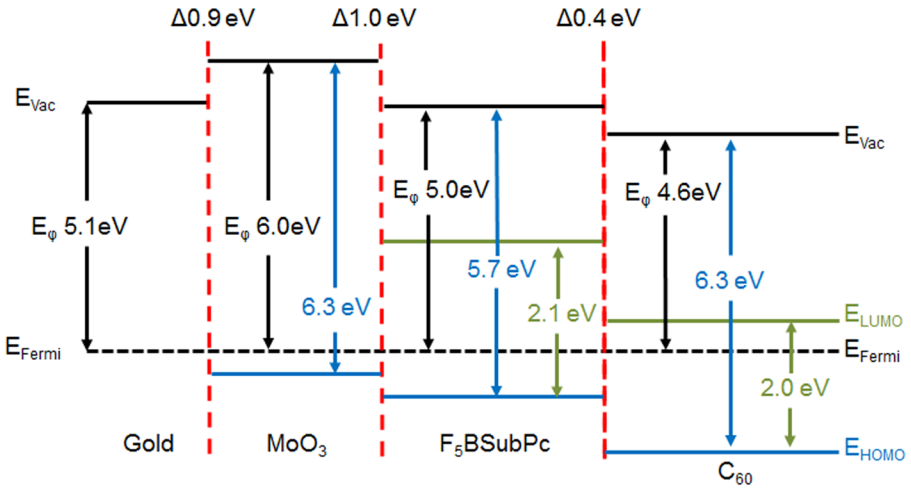

Figure 6. Schematic view of the HOMO levels and local vacuum level shifts for Au/MoO_3/F_5BsubPc/C_{60} heterojunctions, as determined from layer-by-layer vacuum deposition of these materials over a thickness range of ∼10 nm (Figure S1, Supporting Information). Electronic equilibrium is maintained with the spectrometer throughout all deposited layers; hence we show the Fermi energy to be constant throughout all layers. The offset in HOMO energies between the F_5BsubPc and C_{60} layers (0.6 eV) coupled with the assumed bandgap energies for each component (2.1 and 2.0 eV, respectively) leads to an offset in transport LUMO energies ($E^{LUMO}_{F_5} - E^{LUMO}_{C_{60}}$ = ca. 0.7 eV), providing for both the rectification seen in these planar heterojunctions in the dark, and the driving force for exciton dissociation under illumination.

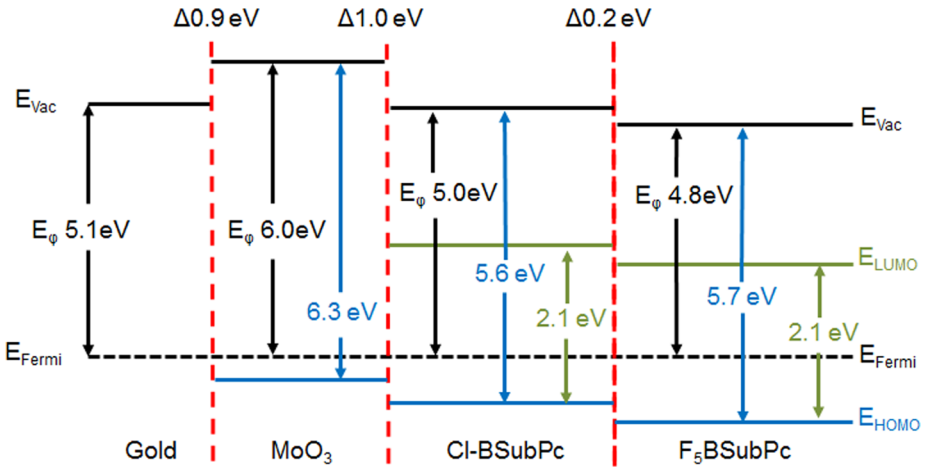

Figure 7. Schematic view of the HOMO levels and local vacuum level shifts for Au/MoO_3/Cl-subPc/F_5BsubPc heterojunctions, as determined from layer-by-layer vacuum deposition of these materials over a thickness range of ~10 nm (Figure S2, Supporting Information). Electronic equilibrium with the spectrometer is maintained throughout all deposited layers, hence the common Fermi energy. The offset in HOMO energies between the Cl-BsubPc and F_5BsubPc (0.1 eV) coupled with the assumed bandgap energies for each component (2.1 eV for each BsubPc) leads to an offset in transport LUMO energies ($E_{Cl}^{LUMO} - E_{F_5}^{LUMO}$ = ca. 0.1 eV).

of the current−voltage response difficult.[23,24,39] Only small shifts in local vacuum level were seen in the UPS spectra of these heterojunctions (Figure S2, Supporting Information), as revealed by shifts in the low kinetic energy edges of the photoemission spectra. Despite the small offsets and the fact that both Cl-BsubPc and F_5BsubPc show Fermi levels that suggest both materials are p-type (relative to C_{60}), reasonable photovoltaic behavior was observed and detailed above for the Cl-BsubPc/F_5BsubPc heterojunction.

OPVs Based on Multiple Electron Donor or Multiple Electron Acceptor Layers. Cascade OPVs have the potential to make use of three organic materials with monotonically decreasing frontier orbital energy levels.[43−46] In one example of an energetically monotonic arrangement of materials, the first layer acts an electron donor layer, the second layer is ambipolar (transports both holes and electrons), and the third layer acts as an electron acceptor layer. This configuration may create two heterojunction regions for exciton dissociation (donor/ambipolar layer and ambipolar layer/acceptor) but the additional heterojunction adds an additional energetic barrier to charge extraction, thus lowering the expected V_{oc}.

As a proof of concept that F_5BsubPc could act as the ambipolar component in a cascade arrangement, we explored two device configurations: ITO/MoO_3 (6 nm)/Cl-BsubPc (10 nm)/F_5BsubPc (x nm)/C_{60} (40 nm)/BCP (10 nm)/Al (100 nm) and ITO/PEN (50 nm)/F_5BsubPc (11 nm)/C_{60} (40 nm)/BCP (10 nm)/Al (100 nm). For the Cl-BsubPc/F_5BsubPc heterojunction, the F_5BsubPc layer was varied between 10, 20 and 40 nm and the OPV device performance was evaluated at each thickness. At 20 and 40 nm, an s-kink was observed in the J/V curve, which is likely attributable to enhanced recombination or charge carrier mobility imbalance in the cascade device architecture.[22] Higher series resistances were also seen at F_5BsubPc thicknesses of 20 and 40 nm. However, at a F_5BsubPc layer thickness of 10 nm, power conversion efficiency of 0.96% and a standard shaped J/V curve was observed (Figure 8). By comparison to the planar bilayer devices described above, this cascade device produces ~50% more photocurrent but has a V_{oc} smaller by ca. 0.3 V (Table 3).

PEN/F_5BsubPc/C_{60} cascade devices also showed the same general performance; higher photocurrents with lower V_{oc}'s. However, in this case less significant gains are observed in overall cell performance perhaps since the PEN/F_5BsubPc/C_{60} cascade device combines two sub cells with strikingly mismatched device performance (V_{oc} of 0.71 V and a J_{sc} of 1.43 mA/cm^2, Table 3). Nonetheless, given these two examples, we can conclude that F_5BsubPc can also function as an ambipolar layer in a cascade arrangement, transporting both electrons and holes while also absorbing light.

CONCLUSIONS

We have demonstrated that F_5BsubPc can function as either an electron-donating/hole-transporting material or an electron-accepting/electron-transporting material in a planar heterojunction organic photovoltaic (PHJ OPV) configuration. Using C_{60} as the electron acceptor and F_5BsubPc as the electron donor, good frontier orbital energy offsets were observed, which are consistent with other high IP donor/C_{60} heterojunctions. OPVs with good rectification, high V_{oc}'s, and reasonable efficiencies were achieved for unoptimized devices. For Cl-BsubPc/F_5BsubPc devices, the offsets in both the HOMO and LUMO energies were measured to be small (ca. 0.1 eV), but good rectification and photovoltaic activity was still achieved. In each case, by deconstructing the devices, we could verify that the rectifying and photocurrent producing interfaces were the F_5BsubPc/C_{60} and Cl-BsubPc/F_5BsubPc interfaces. In each of the device configurations, a strong contribution to the photocurrent was observed at energies below the lowest energy excitonic state. Charge transfer complexes at the donor/acceptor interface are observed by IPCE and are ~1.7 eV for both F_5BsubPc/C_{60} and Cl-BsubPc/F_5BsubPc.

To probe the ambipolarity of F_5BsubPc, we also constructed cascade OPV devices. We demonstrate that F_5BsubPc can function in this role by effectively transporting both holes and electrons while absorbing light albeit only for a specific (and largely unoptimized) F_5BsubPc layer thickness. Our cascade devices produced, on average, higher photocurrent (~50%) presumably due to the two exciton dissociation interfaces but a reduced open circuit voltage (by comparison to a similar donor/acceptor OPV).[47,48]

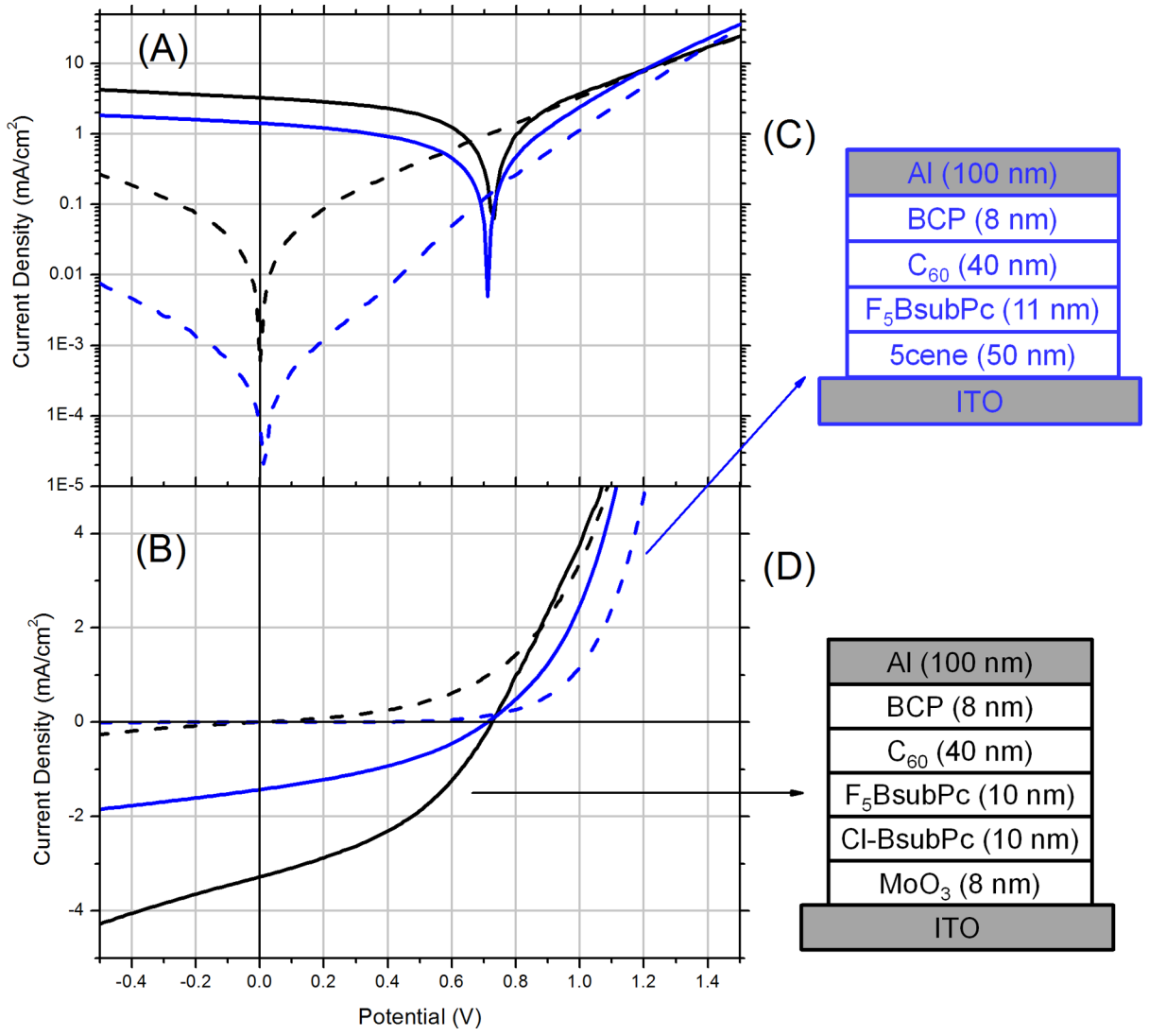

Figure 8. Log (A) and linear (B) dark and illuminated *J*/*V* plots for OPV cascade devices in configurations that require F_5BsubPc to form a heterojunction with PEN backed with C_{60} as the electron transport layer (blue line) or a heterojunction with Cl-BsubPc (black line) backed with C_{60} as the electron transport layer. (C) Device configuration of PEN/F_5BsubPc/C_{60} OPV. (D) Device configuration of Cl-BsubPc/F_5BsubPc/C_{60} OPV.

Table 3. A Comparison between the Cascade OPV Devices ITO/MoO_3/Cl-BsubPc/F_5BsubPc/C_{60}/BCP/Al and ITO/PEN/F_5BsubPc/C_{60}/BCP/Al and Their Comparative Bilayer Devices

donor (nm)	F_5BsubPc (nm)	C_{60} (nm)	V_{oc} (V)	J_{sc} (mA/cm^2)	FF (%)	η (%)
Cl-BsubPc (10)	10	40	0.73	3.28	40.3	0.97
	17	40	1.02	2.03	46.2	0.96
Cl-BsubPc (10)	20		0.98	1.72	44.9	0.76
PEN (50)	29		0.82	0.46	40.8	0.15
PEN (50)	11	40	0.71	1.43	37.2	0.38

F_5BsubPc is a representative of the more general class of phenoxy-BsubPcs. We feel these results further the idea that the field should look beyond the prototypical BsubPc, Cl-BsubPc, and towards the large synthetic variation that is available to phenoxy-BsubPcs. Based on the work outlined herein and our previous work showing the dual functionality of F_5BsubPc in OLEDs,[6,7] we feel phenoxy-BsubPcs may have significant promise across multiple organic electronic device configurations.

EXPERIMENTAL SECTION

ITO coated glass was obtained from Colorado Concept Coating LLC., with a thickness of 150 nm and a sheet resistance of 15 Ω per square (four-point probe). Substrates (1 in. × 1 in.) were cleaned by (1) washing with nanopure water and scrubbing with 10% Triton X-100, (2) sonication in 10% Triton X-100 for 15 min, (3) rinsing and scrubbing with nanopure water, (4) sonication in nanopure water for 15 min, (5) rinsing and scrubbing with 100% ethanol, and (6) sonication in 200 proof ethanol for 15 min. Large area (0.125 cm^2) substrates of 1 in. × 1 in. size were rinsed with 100% ethanol and then patterned with S1813 positive photoresist (Rohm and Haas), followed by exposure, development, etching, and removal of the photoresist to create the necessary patterns for 0.125 cm^2 substrates. Each patterned ITO substrate was etched using aqua regia at a 3:1 ratio at 120 °C for ca. 30 s. The substrates were then cleaned using the six step procedure above and stored in 100% ethanol.

Prior to introduction to the vacuum systems, cleaned ITO substrates were removed from the ethanol solution and dried under a stream of nitrogen. For the plasma treated experiments, the etched substrates were put into a Harrick PDC-32G plasma generator, which

dx.doi.org/10.1021/am404179z | ACS Appl. Mater. Interfaces 2014, 6, 1515−1524

was at ca. 0.4 Torr with dry oxygen etching occurring at 10 min. Detergent solvent cleaned (DSC) ITO was used directly from the stored substrates in ethanol. C_{60}, copper phthalocyanine (CuPc), and pentacene (Mer Corp, Aldrich) were triply sublimed using an in house sublimation system, and bathocuproine (Aldrich) was sublimed twice. Molybdenum oxide (99.99%) was purchased from Aldrich as used as is. The synthesis and purification of pentafluorophenoxy boron subphthalocyanine (F_5BsubPc) has been previously described.[5] In order to ensure high purity, F_5BsubPc was doubly sublimed in a thermal gradient sublimation apparatus. A custom high vacuum deposition system was used to fabricate the various organic photovoltaic test cells used in this study, as described previously.[49−51]

All molecules were thoroughly degassed in the vacuum system prior to use. Aluminum top contacts (Alfa Aesar) were deposited with 99.999% rated material. All molecules used in vacuum deposition were loaded into a Knudsen cell type system and deposited at pressures equal to or lower than 9×10^{-7} Torr. Thin films were deposited at a rate of approximately 0.5 Å/s for organics and 1 Å/s for aluminum, measured with a 10 MHz quartz crystal microbalance (QCM-Newark) and a frequency monitor (Agilent, model 53131A) or a 6 MHz QCM (Lesker) monitored via an Inficon Q-pod QCM monitor. Top contacts were deposited via thermal evaporation and measured with a 6 MHz QCM (Tangydine) and a frequency monitor (Inficon, model 758-500-G1). The OPV devices fabricated in this study were each constructed with pentafluorophenoxy boron subphthalocyanine (F_5BsubPc) as an active material in a variety of planar heterojunction OPVs. F_5BsubPc was paired with other common organic semiconductors so as to limit the number of unknown factors in this investigation. Thicknesses of the active layers were optimized by finding those thicknesses that produced maximum photocurrent and photopotentials and minimized series resistance, maximizing fill-factors. In each case, device performance was reported as an average of more than eight circular 0.019 cm^2 cells. The devices were constructed on a transparent ITO glass electrode with a vacuum deposited 100 nm layer of Al as a top electrode. In each cell, a layer of BCP was used as a barrier to Al migration, which also prevents or reduces the amount of pin-holes and acts as an electron selective interface layer.[52] Cell configurations were either ITO/F_5BsubPc/C_{60}/BCP/Al, ITO/Cl-BsubPc/F_5BsubPc/BCP/Al, or ITO/PEN/F_5BsubPc/BCP/Al.

X-ray photoelectron spectroscopy (XPS) and UV-photoelectron spectroscopy (UPS) were used to probe the interface between each material. Aluminum Kα X-rays at 1486.6 eV were used for XPS measurements, and He(I) was used as the source (21.2 eV) for UPS measurements (Kratos Axis-Ultra spectrophotometer). For UPS measurements, the sample was biased at 10 V to enhance the yield of low kinetic energy electrons.[36,38,53,54] The spot size was 300 μm by 700 μm for XPS and 1 mm to 3 mm for UPS measurements. The work function of clean Au (Alfa Aesar) was verified to be ca. 5.1 ± 0.1 eV and to set the kinetic energy of photoelectrons emitted at the Fermi energy for Au, which was assumed constant for all subsequent ITO/organic heterojunctions; that is, we assume electronic equilibrium between the sample and the spectrometer.[36] Throughout the data collection process, photoemission from the gold Fermi level varied from 30.7 to 34 eV (absolute kinetic energy) for sputter cleaned gold substrates. Gold was polished to a mirror finish and soaked in piranha for 24 h and subsequently argon sputtered prior to the experiment. Molecules were deposited on ITO (Colorado Concept Coating LLC) in an attached high vacuum deposition system where the rate was monitored using a quartz crystal monitor (Agilent 53131A) and custom designed quartz oscillator (QCM-Newark) where depositions of sub-angstrom per second are possible on either gold or ITO substrates. The temperature was controlled by an Omega CN76000 temperature driver/controller.

For testing devices, a custom made current−voltage (J/V) system was used to test six devices per substrate for large area (0.125 cm^2) devices and 25 per substrate for small area (0.019 cm^2). J/V measurements were performed in a nitrogen filled glovebox (Mbraun Labmaster) where water and oxygen levels were below 0.1 ppm. A 300 W xenon arc lamp (Newport) that is current controlled was used as the light source. The beam path from the source to the sample was filtered using an AM 1.5 filter (MellesGriot) to simulate the solar spectrum. The filtered light was then optically diffused using an engineered diffuser with an output of 40° (Newport). The power density at the surface of the devices was tuned with a flat response thermopile (Newport) and cross checked with a calibrated silicon photodiode (Newport, model 818-SL with OD3 Attenuator) to get 100 mW/cm^2. The potential applied to the device was swept using a source meter (Keithley 2400) and in-house software (National Instruments Labview 8.2). The potential was swept from −1.00 to 1.50 V using a 5.00 mV step starting from the negative potential. Absorbance measurements were carried out with a UV/visible spectrophotometer (Agilent Technologies, model 8453). Incident and absorbed power conversion efficiency (IPCE and APCE) measurements were acquired in an in-house fabricated hermetically sealed unit. A 300 W xenon arc lamp (Newport) was used as the light source. The 256 Hz modulated light (Stanford Research) was passed through an automated monochromator (Newport, Cornerstone 130), where the data was acquired at 4 nm intervals. Incident power though the monochromator and custom optics setup was measured with a silicon photodiode (Newport model 818-SL), while device measurements were acquired at short-circuit. The resulting signal was fed to a lock-in amplifier (EG&G model 5209), while the output was fed into an in-house data acquisition system (National Instruments Labview 8.2). The APCE values have been normalized because refractive indices and reflection off the back electrode were not taken into account.

■ ASSOCIATED CONTENT

Ⓢ Supporting Information

Full ultraviolet photoelectron spectroscopy data of the F_5BsubPc/C_{60} and Cl-BsubPc/F_5BsubPc interface, large area device performance of the Cl-BsubPc/F_5BsubPc device, and Cl-BsubPc Schottky device performance. This material is available free of charge via the Internet at http://pubs.acs.org.

■ AUTHOR INFORMATION

Corresponding Authors

*E-mail: nra@email.arizona.edu.
*E-mail: tim.bender@utoronto.ca.

Notes

The authors declare no competing financial interest.

■ ACKNOWLEDGMENTS

This research was supported as part of the Center for Interface Science: Solar Electric Materials (CISSEM), an Energy Frontier Research Center funded by the U.S. Department of Energy, Office of Science, Office of Basic Energy Sciences under Award No. DE-SC0001084 (JLG, KXS, NRA). We thank the National Science and Engineering Research Council of Canada (NSERC) for supporting G.E. Morse with a Canadian Graduate Scholarship and the Michael Smith Foreign Travel Supplement to fund this collaboration between the University of Toronto and the University of Arizona.

■ REFERENCES

(1) Shun-Wei, L.; Chin-Ti, C.; Jiun-Haw, L. Presented at the Nanoelectronics Conference (INEC), 2011 IEEE 4th International, 21-24 June 2011; 2011, 1-2.
(2) Liu, S.-W.; Lin, C.-F.; Lee, C.-C.; Su, W.-C.; Chen, C.-T.; Lee, J.-H. *J. Electrochem. Soc.* **2012**, *159* (2), H191−H194.
(3) Jiang, H. *Macromol. Rapid Commun.* **2010**, *31* (23), 2007−2034.
(4) Mutolo, K. L.; Mayo, E. I.; Rand, B. P.; Forrest, S. R.; Thompson, M. E. *J. Am. Chem. Soc.* **2006**, *128* (25), 8108−8109.
(5) Gommans, H.; Aernouts, T.; Verreet, B.; Heremans, P.; Medina, A.; Claessens, C. G.; Torres, T. *Adv. Funct. Mater.* **2009**, *19* (21), 3435−3439.

(6) Sullivan, P.; Duraud, A.; Hancox, I.; Beaumont, N.; Mirri, G.; Tucker, J. H. R.; Hatton, R. A.; Shipman, M.; Jones, T. S. *Adv. Energy Mater.* **2011**, *1* (3), 352−355.
(7) Morse, G. E.; Helander, M. G.; Maka, J. F.; Lu, Z. H.; Bender, T. P. *ACS Appl. Mater. Interfaces* **2010**, *2* (7), 1934−1944.
(8) Helander, M. G.; Morse, G. E.; Qiu, J.; Castrucci, J. S.; Bender, T. P.; Lu, Z. H. *ACS Appl. Mater. Interfaces* **2010**, *2* (11), 3147−3152.
(9) Díaz, D. D.; Bolink, H. J.; Cappelli, L.; Claessens, C. G.; Coronado, E.; Torres, T. *Tetrahedron Lett.* **2007**, *48* (27), 4657−4660.
(10) Yasuda, T.; Tsutsui, T. *Mol. Cryst. Liq. Cryst.* **2006**, *462* (1), 3−9.
(11) Castrucci, J. S.; Helander, M. G.; Morse, G. E.; Lu, Z. H.; Yip, C. M.; Bender, T. P. *Cryst. Growth Des.* **2012**, *12* (3), 1095−1100.
(12) Morse, G. E.; Castrucci, J. S.; Helander, M. G.; Lu, Z. H.; Bender, T. P. *ACS Appl. Mater. Interfaces* **2011**, *3* (9), 3538−3544.
(13) Beaumont, N.; Cho, S. W.; Sullivan, P.; Newby, D.; Smith, K. E.; Jones, T. S. *Adv. Funct. Mater.* **2012**, *22*, 561−566.
(14) Morse, G. E.; Bender, T. P. *ACS Appl. Mater. Interfaces* **2012**, *4* (10), 5055−5068.
(15) Gommans, H.; Cheyns, D.; Aernouts, T.; Girotto, C.; Poortmans, J.; Heremans, P. *Adv. Funct. Mater.* **2007**, *17* (15), 2653−2658.
(16) Hancox, I.; Sullivan, P.; Chauhan, K.; Beaumont, N.; Rochford, L.; Hatton, R.; Jones, T. *Org. Electron.* **2010**, *11* (12), 2019−2025.
(17) Kroger, M.; Hamwi, S.; Meyer, J.; Riedl, T.; Kowalsky, W.; Kahn, A. *Appl. Phys. Lett.* **2009**, *95* (12), 3.
(18) Kroger, M.; Hamwi, S.; Meyer, J.; Riedl, T.; Kowalsky, W.; Kahn, A. *Org. Electron.* **2009**, *10* (5), 932−938.
(19) Hamwi, S.; Meyer, J.; Kröger, M.; Winkler, T.; Witte, M.; Riedl, T.; Kahn, A.; Kowalsky, W. *Adv. Funct. Mater.* **2010**, *20* (11), 1762−1766.
(20) Tress, W.; Petrich, A.; Hummert, M.; Hein, M.; Leo, K.; Riede, M. *Appl. Phys. Lett.* **2011**, *98*, No. 063301.
(21) Tress, W.; Leo, K.; Riede, M. *Phys. Rev. B* **2012**, *85*, No. 155201.
(22) Mandoc, M. M.; Koster, L. J. A.; Blom, P. W. M. *Appl. Phys. Lett.* **2007**, *90*, No. 133504.
(23) Rand, B. P.; Burk, D. P.; Forrest, S. R. *Phys. Rev. B* **2007**, *75* (11), No. 115327.
(24) Forrest, S. R. *MRS Bull.* **2005**, *30* (1), 28−32.
(25) Potscavage, W. J.; Yoo, S.; Kippelen, B. *Appl. Phys. Lett.* **2008**, *93*, No. 193308.
(26) Zhang, M.; Ding, H.; Gao, Y.; Tang, C. *Appl. Phys. Lett.* **2010**, *96* (18), No. 183301.
(27) Shrotriya, V.; Li, G.; Yao, Y.; Moriarty, T.; Emery, K.; Yang, Y. *Adv. Funct. Mater.* **2006**, *16* (15), 2016−2023.
(28) Pandey, R.; Holmes, R. J. *Adv. Mater.* **2010**, *22* (46), 5301−5305.
(29) Gommans, H.; Verreet, B.; Rand, B. P.; Muller, R.; Poortmans, J.; Heremans, P.; Genoe, J. *Adv. Funct. Mater.* **2008**, *18* (22), 3686−3691.
(30) Graham, K. R.; Erwin, P.; Nordlund, D.; Vandewal, K.; Li, R.; Ngongang Ndjawa, G. O.; Hoke, E. T.; Salleo, A.; Thompson, M. E.; McGehee, M. D.; Amassian, A. *Adv. Mater.* **2013**, *25*, 6076−6082.
(31) Verreet, B.; Rand, B. P.; Cheyns, D.; Hadipour, A.; Aernouts, T.; Heremans, P.; Medina, A.; Claessens, C. G.; Torres, T. *Adv. Energy Mater.* **2011**, *1* (4), 565−568.
(32) Griffith, O. L.; Anthony, J. E.; Jones, A. G.; Lichtenberger, D. L. *J. Am. Chem. Soc.* **2009**, *132* (2), 580−586.
(33) Jurchescu, O. D.; Baas, J.; Palstra, T. T. M. *Appl. Phys. Lett.* **2004**, *84* (16), 3061−3063.
(34) Yoo, S.; Potscavage, W. J., Jr.; Domercq, B.; Han, S.-H.; Li, T.-D.; Jones, S. C.; Szoszkiewicz, R.; Levi, D.; Riedo, E.; Marder, S. R.; Kippelen, B. *Solid State Electron.* **2007**, *51* (10), 1367−1375.
(35) Pakhomov, G.; Travkin, V. V.; Bogdanova, A. Y.; Guo, T. F. *J. Porphyrins Phthalocyanines* **2008**, *12* (11), 1182−1186.
(36) Armstrong, N. R.; Wang, W. N.; Alloway, D. M.; Placencia, D.; Ratcliff, E.; Brumbach, M. *Macromol. Rapid Commun.* **2009**, *30* (9-10), 717−731.
(37) Ishii, H.; Sugiyama, K.; Ito, E.; Seki, K. *Adv. Mater.* **1999**, *11* (8), 605−625.
(38) Hwang, J.; Wan, A.; Kahn, A. *Mater. Sci. Eng., R: Reports* **2009**, *64* (1-2), 1−31. (c) Cahen, D.; Kahn, A. *Adv. Mater.* **2003**, *15* (4), 271−277.
(39) Tang, C. W. *Appl. Phys. Lett.* **1986**, *48* (2), 183−185.
(40) Zhang, M. L.; Wang, H.; Tang, C. W. *Appl. Phys. Lett.* **2010**, *97* (14), No. 143503.
(41) Alloway, D. M.; Armstrong, N. R. *Appl. Phys. A: Mater. Sci. Process.* **2009**, *95* (1), 209−218.
(42) Ratcliff, E. L.; Zacher, B.; Armstrong, N. R. *J. Phys. Chem. Lett.* **2011**, 1337−1350.
(43) Zhang, G.; Li, W.; Chu, B.; Chen, L.; Yan, F.; Zhu, J.; Chen, Y.; Lee, C. S. *Appl. Phys. Lett.* **2009**, *94* (14), No. 143302.
(44) Ichikawa, M.; Takekawa, D.; Jeon, H. G.; Banoukepa, G. D. R. *Org. Electron.* **2013**, *14* (3), 814−820.
(45) Schlenker, C. W.; Barlier, V. S.; Chin, S. W.; Whited, M. T.; McAnally, R. E.; Forrest, S. R.; Thompson, M. E. *Chem. Mater.* **2011**, *23* (18), 4132−4140.
(46) Chen, M. C.; Liaw, D. J.; Huang, Y. C.; Wu, H. Y.; Tai, Y. *Sol. Energy Mater. Sol. Cells* **2011**, *95* (9), 2621−2627.
(47) Yuen, A. P.; Hor, A.-M.; Preston, J. S.; Klenkler, R.; Bamsey, N. M.; Loutfy, R. O. *Appl. Phys. Lett.* **2011**, *98* (17), No. 173301.
(48) Huang, J.-H.; Velusamy, M.; Ho, K.-C.; Lin, J.-T.; Chu, C.-W. *J. Mater. Chem.* **2010**, *20* (14), 2820−2825.
(49) Wang, W.; Placencia, D.; Armstrong, N. R. *Org. Electron.* **2011**, *12*, 383−393.
(50) Placencia, D.; Wang, W. N.; Gantz, J.; Jenkins, J. L.; Armstrong, N. R. *J. Phys. Chem. C* **2011**, *115* (38), 18873−18884.
(51) Placencia, D.; Wang, W. N.; Shallcross, R. C.; Nebesny, K. W.; Brumbach, M.; Armstrong, N. R. *Adv. Funct. Mater.* **2009**, *19* (12), 1913−1921.
(52) Wang, Y.-M.; Teng, F.; Zhou, Q.-C.; Wang, Y.-S. *Appl. Surf. Sci.* **2006**, *252* (6), 2355−2359.
(53) Schlaf, R.; Parkinson, B.; Lee, P.; Nebesny, K.; Armstrong, N. *J. Phys. Chem. B* **1999**, *103* (15), 2984−2992.
(54) Alloway, D. M.; Graham, A. L.; Yang, X.; Mudalige, A.; Colorado, R.; Wysocki, V. H.; Pemberton, J. E.; Randall Lee, T.; Wysocki, R. J.; Armstrong, N. R. *J. Phys. Chem. C* **2009**, *113* (47), 20328−20334.